Multiple Model Dynamic Mode Decomposition for Flowfield and Model Parameter Estimation

Alexandros Tsolovikos *, Saikishan Suryanarayanan †, Efstathios Bakolas ‡, and David Goldstein §
The University of Texas at Austin, Austin, Texas 78712-1221

In this work, we present a method for estimating the unsteady flowfield of a fluid system with unknown model parameters (such as angle of attack or Reynolds number) in real time from a limited number of sensor measurements using a "bank" of Dynamic Mode Decomposition (DMD) models. First, a set of DMD models is computed at sample values of the model parameter. Then, a bank of Kalman filters is run for each one of the models, yielding a state estimate for each one of the DMD models and, thus, a corresponding flowfield estimate. Finally, the minimum mean-squared error (MMSE) estimate of the actual flowfield is computed as a weighted sum of the individual flowfield estimates from each model, where the weights are the likelihood of each model being the correct one given current and past measurements, under the Multiple Model Kalman Filter (MMKF) framework. The performance of the proposed approach to estimating the flowfield of a system with varying parameters is demonstrated in simple flow settings: a Blasius boundary layer at discrete adverse pressure gradients and a flat plate at different angles of attack.

I. Introduction

ESTIMATING the unsteady flowfield in practical flow settings, such as around airfoils, is a useful and, often, necessary step in evaluating the performance of such systems and controlling them. For instance, the unsteady flow structures around an airfoil may depend on the (possibly varying) angle of attack and Reynolds number and directly affect the lift and drag coefficients. Fluid flows are infinite-dimensional, nonlinear, and, often, chaotic dynamical systems governed by a set of partial differential equations – the Navier-Stokes (NS) equations – which are intractable to solve in real time. For that reason, any attempt to estimate the state of such a system requires a model-reduction step (e.g. if a high-dimensional dynamical model, such as the linearized NS equations [1], is available) and/or a system identification step (if only numerical or experimental data are available) [2].

The infinite-dimensional states (e.g. velocity, pressure, or vorticity) of fluid flows are commonly discretized in space at a set of fixed grid points, leading to a finite, but high-dimensional state space. A number of model reduction techniques for discovering low-dimensional patterns that describe the evolution of such systems have appeared in the literature [3–8].

One popular model reduction method is *proper orthogonal decomposition* (POD), also known as Principal Component Analysis (PCA). First introduced in the fluid mechanics community by Lumley [3], POD computes the singular value decomposition (SVD) of a collection of flow snapshots (e.g. the velocities at a set of grid points) and identifies a subspace on which the discretized flow equations or measurements are projected [9]. POD modes are optimal in the $\mathcal{L}_2$-norm sense and, therefore, describe flow structures based on their energy content. However, low-energy modes can have a large influence on the evolution of fluid flows [2]. Variations of POD, such as *balanced proper orthogonal decomposition* (BPOD) [4], have also been proposed. BPOD retains the most controllable and observable modes of the flow, producing models that are suitable for both control and estimation. However, this method requires data from impulse responses of the primary system, as well as from the adjoint system, for which the equations need to be known. Another commonly used system identification method is the eigensystem realization algorithm (ERA) [5], a subspace system identification method that extracts linear state-space models from impulse response data only. This method is attractive, since it can be used when only experimental data are available. In fact, it was shown in [10] that ERA computes the same state-space model as BPOD without the need for adjoint response data, but does not compute the BPOD modes. However, impulse response data may not be easy to obtain. A common solution to this restriction is

*Ph.D. Candidate, Aerospace Engineering and Engineering Mechanics; tsolovikos@utexas.edu; Student Member (Corresponding Author).
†Research Associate, Aerospace Engineering and Engineering Mechanics; Member.
‡Associate Professor, Aerospace Engineering and Engineering Mechanics; Senior Member.
§Professor, Aerospace Engineering and Engineering Mechanics; Associate Fellow.

to use the observer/Kalman filter identification (OKID) technique to extract the impulse response of a system from input-output data of random inputs [5].

Dynamic mode decomposition (DMD), first introduced in [7] and [6], has been a popular model reduction method in recent years, used as an alternative or as complementary to POD for extracting dynamical features of flows purely from time-resolved snapshot data. DMD modes represent flow structures with coherent dynamics, i.e. a specific frequency and decay rate, instead of being characterized by their energy content. A number of extensions to the original DMD algorithm have been proposed for handling systems with control inputs [8], time-varying systems [11], noisy datasets [12, 13], and streaming datasets with a large number of snapshots [14], just to name a few. A probabilistic version of DMD has also been proposed in [15], while the connection of DMD to Koopman spectral analysis [16] has inspired a number of extensions to systems where the dynamics cannot be sufficiently described by a linear system [17, 18].

One of the weaknesses of DMD is that the dynamic modes do not have an objective ranking, unlike POD modes which are ranked based on their energy content, making the selection of the most important DMD modes nontrivial. A number of methods for choosing the DMD modes have been proposed, such as optimized DMD [19], optimal mode decomposition [20], and sparsity-promoting DMD (DMDsp) [21]. *Sparsity-promoting* DMD, first introduced by Jovanovic et al. [21], is a particularly attractive method for truncating the DMD modes in a systematic way by solving a convex optimization problem with a performance index that includes a sparsity-promoting term. Inspired by DMDsp and its extension to systems with inputs in [22], the authors reformulated sparsity-promoting DMD as a one-time-step-ahead least-squares optimization, similar to [23], that can also include the effects of control inputs [24]. This reformulation of DMDsp was recently used for flow control applications [25].

The goal of this work is to estimate in real time the full flowfield for systems with (continuously or discretely) *varying* model parameters, when the full flowfield for different model parameters is available at training time but only a limited number of sensor measurements are available at test time, while the model parameters are also unknown. As an illustrative example, consider an aircraft flying in gusty conditions, where the flow around the wing depends on the angle of attack (the model parameter) which can vary and is perhaps hard to measure independently in such conditions. We assume that for a fixed model parameter the underlying system can be sufficiently approximated by a Dynamic Mode Decomposition model and, therefore, an optimal linear estimator – i.e. a Kalman Filter – can be used as the base estimator. Kalman filters have been previously used in combination with DMD models for flowfield estimation [26], flow control [24], and denoising the DMD modes [27, 28]. In the context of Koopman operators, Kalman filters have also been used for the design of linear observers for nonlinear systems [29]. In this work, the idea of estimating a high-dimensional flowfield from limited sensor measurements is extended to systems with varying model parameters, where a single DMD model is insufficient to describe the system at different parameter values. In order to expand the applicability of linear filters for flowfield estimation, we use a *bank* of DMD models at different values of the model parameters and compute the minimum mean-squared error (MMSE) estimate of the flowfield from a limited number of sensor measurements using a Multiple Model Kalman Filter (MMKF) [30, 31] that "balances" or "weights" the contribution of each model to the MMSE-estimated flowfield based on the probability of each model being correct given the history of measurements. In addition, the unknown model parameter can also be inferred from the probabilities of each model: the most probable value of the parameter is simply the one on which the most probable DMD model was trained on.

Numerical examples demonstrating the basic idea of flowfield estimation from limited measurements with unknown parameters using a bank of DMD models and MMKF is demonstrated in simple flow settings: 1) a Blasius boundary layer at various adverse pressure gradients and 2) the flow around a flat plate at time-varying angles of attack (AoA).

The rest of the paper is organized as follows. In Section II, we briefly describe the process of computing a single sparsity-promoting DMD model from snapshot data. In Section III we formulate the Kalman filter estimator for a single DMD model. Section IV presents multiple model DMD for flowfield estimation – the main contribution of this work. Numerical examples are presented in Section V. We conclude with remarks and directions for future research in Section VI.

II. System Identification Using Dynamic Mode Decomposition

The motion of a fluid is generally described by a set of nonlinear partial differential equations – the Navier Stokes equations – that are infinite dimensional and not easily amenable to standard real-time estimation techniques, such as the celebrated Kalman filter [31]. For that reason, it is desirable to have an approximate low-dimensional linear model that can be identified from numerical or experimental data. Such a model can be easily derived using Dynamic Mode Decomposition (DMD), and its variants, such as the sparsity-promoting DMD.

Before moving to the case of varying model parameters, we first present the process of estimating a high-dimensional flowfield from limited measurements (e.g. wall-mounted sensors) using a *single* DMD model, similar to [26] and [24]. Toward that goal, we begin by presenting the standard DMD and its sparsity-promoting variant (DMDsp), first developed in [21] and reformulated in [24] as a one-time-step-ahead least-squares optimization, similar to [23], that can also include the effects of control inputs.

A. Dynamic Model Decomposition

Let the dynamics of the high-dimensional system be described by an unknown (and, generally, nonlinear) function $\mathbf{f}(\cdot) : \mathbb{R}^{n_y} \to \mathbb{R}^{n_y}$, such that

$$\mathbf{y}_{k+1} = \mathbf{f}(\mathbf{y}_k), \tag{1}$$

where $\mathbf{y}_k \in \mathbb{R}^{n_y}$ is the state of the high-dimensional system (e.g. the velocity components at a set of grid points) at time step k and $n_y \ll 1$.

Assume that we have a set of training data pairs $\mathcal{D} = \{(\mathbf{y}^{(i)}, \mathbf{f}(\mathbf{y}^{(i)})) : i = 1, \ldots, p\}$ that are stacked as the columns of the following "data matrices"

$$Y = \begin{bmatrix} \mathbf{y}^{(1)} & \cdots & \mathbf{y}^{(p)} \end{bmatrix} \in \mathbb{R}^{n_y \times p}, \tag{2a}$$

$$Y' = \begin{bmatrix} \mathbf{f}(\mathbf{y}^{(1)}) & \cdots & \mathbf{f}(\mathbf{y}^{(p)}) \end{bmatrix} \in \mathbb{R}^{n_y \times p}, \tag{2b}$$

with p denoting the number of available pairs and $p \ll n_y$.

Since the state $\mathbf{y}$ is high-dimensional, identifying a linear model in $\mathbb{R}^{n_y}$ can be computationally intractable. Instead, we seek an optimal (in the $\mathcal{L}_2$-norm sense) low-dimensional subspace to project the high-dimensional state using proper orthogonal decomposition (POD). The singular value decomposition of Y,

$$Y = U\Sigma V^\top, \tag{3}$$

yields the POD modes – which are the orthonormal eigenvectors of $YY^\top$ – as the columns of $U \in \mathbb{R}^{n_y \times p}$, arranged by their energy content, i.e. their singular value. A common choice for the low-dimensional space is the range space of $U_q \in \mathbb{R}^{n_y \times q}$ formed by the first q most energetic POD modes. The high-dimensional state $\mathbf{y}$ is then projected onto the range-space of U_q, yielding a low-dimensional (reduced-order) state $\boldsymbol{\eta} \in \mathbb{R}^q$, where

$$\boldsymbol{\eta}_k = U_q^\top \mathbf{y}_k \tag{4}$$

at time step k. The original state $\mathbf{y}$ (i.e. the full flowfield) can be approximated as

$$\mathbf{y}_k = U_q \boldsymbol{\eta}_k + \boldsymbol{\epsilon}_k, \tag{5}$$

with $\boldsymbol{\epsilon}_k \in \mathbb{R}^{n_y}$ denoting the approximation error.

If we assume a linear form for the reduced-order dynamics,

$$\boldsymbol{\eta}_{k+1} = F\boldsymbol{\eta}_k, \tag{6}$$

we can fit $F \in \mathbb{R}^{q \times q}$ to the data set $\mathcal{D}$ in a least-squares sense as

$$F = (U_q^\top Y')(U_q^\top Y)^\dagger, \tag{7}$$

where $\dagger$ denotes the Moore-Penrose inverse. The DMD modes can then be extracted by bringing Eq. 7 in *complex* modal form. Assuming that F has a set of linearly-independent eigenvectors $\{\mathbf{w}_1, \ldots, \mathbf{w}_q\}$, we can fit

$$FW = W\Lambda, \tag{8}$$

where $W \in \mathbb{C}^{q \times q}$ is the nonsingular matrix containing the right eigenvectors of F, $\Lambda = \text{diag}\{\lambda\} \in \mathbb{C}^{q \times q}$, and $\lambda = \begin{bmatrix} \lambda_1 & \cdots & \lambda_q \end{bmatrix}^\top \in \mathbb{C}^q$ is the vector of eigenvalues of F. Setting $\boldsymbol{\eta}_k = W\boldsymbol{\psi}_k$, we get Eq. 7 in modal form,

$$\boldsymbol{\psi}_{k+1} = \Lambda\boldsymbol{\psi}_k, \tag{9}$$

where $\boldsymbol{\psi}_k \in \mathbb{C}^{n_y}$ is the complex vector of the amplitudes of the DMD modes at time step k. The high-dimensional state $\mathbf{y}_k$ can now be approximated as

$$\mathbf{y}_k \approx \Phi \boldsymbol{\psi}_k \tag{10}$$

where $\Phi = U_q W \in \mathbb{C}^{n_y \times q}$ and the i-th column of Φ, which is denoted as $\boldsymbol{\phi}_i \in \mathbb{C}^{n_y}$, is the i-th DMD mode corresponding to the eigenvalue λ_i.

B. Sparsity-Promoting Dynamic Mode Decomposition

The DMD modes, $\boldsymbol{\phi}_i$, decompose the flowfield based on the frequency and decay rate of the corresponding eigenvalue, λ_i. However, the number of DMD modes that we have is equal to the number of POD modes we chose to keep – a choice based on the approximation error or "energy content" of the first few POD modes. However, energetic POD modes are not necessarily dynamically important.

In order to determine the most important DMD modes, sparsity-promoting DMD (DMDsp) was developed in [21]. Recently, (DMDsp) was reformulated in [24] as a one-time-step-ahead least-squares optimization, similar to [23], that can also include the effects of control inputs and does not require the data to come from the same time sequence.

Using the approach in [24], we truncate the DMD modes by weighting the contribution of each mode to the dynamics with a scalar weight α_i

$$\mathbf{y}_{k+1} = \sum_{i=1}^{q} \alpha_i \boldsymbol{\phi}_i \lambda_i \psi_{i,k} + \boldsymbol{\varepsilon}_k, \tag{11}$$

where $\psi_{i,k}$ is the $i-$th component of vector $\boldsymbol{\psi}_k$. A sparse representation of $\boldsymbol{\alpha} = \begin{bmatrix} \alpha_1 & \dots & \alpha_q \end{bmatrix}^\top$ is obtained by minimizing the error $\boldsymbol{\varepsilon}_k$ for the training data, along with a regularization or sparsity-promoting term $\|\boldsymbol{\alpha}\|_0$. In particular, we minimize the cost function

$$J_{\mathrm{LS}}(\boldsymbol{\alpha}) := \|Y' - \Phi \mathrm{diag}\{\boldsymbol{\alpha}\} \Lambda \Phi^\dagger Y\|_{\mathrm{F}}^2 + \rho \|\boldsymbol{\alpha}\|_0, \tag{12}$$

where ρ balances the importance of sparsity versus approximation and $\|\cdot\|_{\mathrm{F}}$ denotes the Frobenius norm. The sparsity-promoting term $\|\boldsymbol{\alpha}\|_0$ is approximated by the reweighted $\mathscr{L}_1$ norm [32], making the least-squares problem convex.

The sparse solution to the preceding problem is a vector $\boldsymbol{\alpha} = \begin{bmatrix} \alpha_1 & \cdots & \alpha_q \end{bmatrix}^\top \in \mathbb{R}^q$, with only $n_x < q$ non-zero terms. The states of $\boldsymbol{\psi}_k$ that correspond to $\alpha_i = 0$ are truncated, resulting in an n_x-dimensional state-space model containing only the dynamically relevant DMD modes. After transforming the truncated state-space model from *complex* to *real* modal form, we obtain the sparse reduced-order linear model

$$\mathbf{x}_{k+1} = A\mathbf{x}_k \tag{13a}$$

$$\mathbf{y}_k = \Theta \mathbf{x}_k \tag{13b}$$

where $\mathbf{x}_k \in \mathrm{R}^{n_x}$ is the sparse reduced-order state, $A \in \mathbb{R}^{n_x \times n_x}$, and $\Theta \in \mathbb{R}^{n_y \times n_x}$ is the output matrix containing the real and imaginary parts of the most important DMD modes, with $n_x < q \ll n_y$. For more details, the reader is referred to [24].

III. Flowfield Estimation Using Dynamic Mode Decomposition

In practical flow control applications, full flowfield measurements are generally expensive to obtain (e.g. through numerical simulations or experimental measurements) and only few such measurements might be available during the training process. On the other hand, real-time measurements from a limited number of sensors, such as wall-mounted pressure or shear-stress sensors, are more easily available upon deployment. Using the full flowfield "training" measurements, we can obtain a DMD model and then estimate the full flowfield from a small set of sensors using a Kalman filter, as presented in [26] and [24].

At each time step k, assume that only some of the elements of the full state $\mathbf{y}_k$ are available as measurements, i.e. $\mathbf{z}_k = E_z \mathbf{y}_k$, where $\mathbf{z}_k \in \mathbb{R}^{n_z}$ is the measurement vector containing only n_z of the n_y elements of $\mathbf{y}_k$, $E_z \in \mathbb{R}^{n_z \times n_x}$ is the matrix that truncates the elements of $\mathbf{y}_k$ that are not measured, and $n_z \ll n_y$. If we define $C = E_z \Theta$, the measurement $\mathbf{z}_k$ can be related to the state $\mathbf{x}_k$ via

$$\mathbf{z}_k = C\mathbf{x}_k. \tag{14}$$

A. Error Estimation

Similar to [26], assume that the stochastic form of model (13a) and the output equation (14) can be written as

$$\mathbf{x}_{k+1} = A\mathbf{x}_k + \mathbf{w}_k, \tag{15a}$$

$$\mathbf{z}_k = C\mathbf{x}_k + \mathbf{v}_k, \tag{15b}$$

where $\mathbf{w}_k \in \mathbb{R}^{n_x}, \mathbf{w}_k \sim \mathcal{N}(0, Q)$ is the process noise (e.g. due to modeling errors) and $\mathbf{v}_k \in \mathbb{R}^{n_z}, \mathbf{v}_k \sim \mathcal{N}(0, R)$ is the measurement noise. Both the process and measurement noises are assumed to be sequences of independent and identically distributed Gaussian random variables with covariances $Q \in \mathbb{R}^{n_x \times n_x}$ and $R \in \mathbb{R}^{n_z \times n_z}$ (symmetric positive definite matrices) that are constant and are chosen based on the modeling errors resulting from DMDcsp as follows: If a full flowfield measurement $\mathbf{y}_k$ is available, the best estimate for $\mathbf{x}_k$ is

$$\hat{\mathbf{x}}_k = \Theta^{\dagger}\mathbf{y}_k. \tag{16}$$

Given (16) and the stochastic linear state space model (15a) - (15b), the best estimate of the process and measurement noise, when the full flowfields $\mathbf{y}_k$ and $\mathbf{y}_{k+1}$ and the limited measurement $\mathbf{z}_k$ are known, is

$$\mathbf{w}_k = \Theta^{\dagger}\mathbf{y}_{k+1} - A\Theta^{\dagger}\mathbf{y}_k, \tag{17}$$

$$\mathbf{v}_k = \mathbf{z}_k - C\Theta^{\dagger}\mathbf{y}_k. \tag{18}$$

Thus, the covariances $Q = \mathbb{E}\left[\mathbf{w}_k\mathbf{w}_k^{\top}\right]$ and $R = \mathbb{E}\left[\mathbf{v}_k\mathbf{v}_k^{\top}\right]$, can be directly estimated from the ensembles of full flowfield data $\mathcal{D}$ that are available during the design process.

Note that the additive Gaussian white noise processes in (15a) and (15b) are chosen as a model for the approximation error of the identified DMD model, even if the actual error at each time step does not correspond to a realization of a sequence of independent and identically distributed random vectors, but one that follows deterministic – albeit too complicated to model – dynamics. However, for additional robustness to measurement noise, we set $R = \mathbb{E}\left[\mathbf{v}_k\mathbf{v}_k^{\top}\right] + \sigma_z I$, where σ_z is the standard deviation of the expected measurement noise.

B. Kalman Filter

With the covariances of the process and measurement noises computed, the well-known Kalman filter [31] can now be applied to estimate the amplitudes of the DMD modes $\mathbf{x}_k$, as well as the full flowfield $\mathbf{y}_k$, from the limited measurements $\mathbf{z}_k$. For an initial guess $\hat{\mathbf{x}}_0$ of the state estimate and P_0 of the state covariance, given the previous estimates $\hat{\mathbf{x}}_{k-1}$, P_{k-1}, and the measurement $\mathbf{z}_k$, the state $\mathbf{x}_k$ can be estimated using the following steps:

1) State propagation:

$$\hat{\mathbf{x}}_k^- = A\hat{\mathbf{x}}_{k-1}$$
$$P_k^- = AP_{k-1}A^{\top} + Q_e$$

2) Measurement update:

$$K_k = P_k^- C^{\top}\left[CP_k^- C^{\top} + R_e\right]^{-1}$$
$$\hat{\mathbf{x}}_k = \hat{\mathbf{x}}_k^- + K_k\left[\mathbf{z}_k - C\hat{\mathbf{x}}_k^-\right]$$
$$P_k = \left[I - K_k C\right]P_k^-,$$

where $\mathbf{x}_k^-$ is the a priori state estimate, P_k^- the a priori state covariance, K_k the Kalman gain, $\hat{\mathbf{x}}_k$ the updated (a posteriori) state estimate, and P_k the updated state covariance. Thus, for an observable pair (A, C), the DMD mode amplitudes $\mathbf{x}_k$ can be estimated from limited measurements $\mathbf{z}_k$ without the need to know the entire snapshot $\mathbf{y}_k$. The full flowfield can then be estimated from the limited measurements as

$$\hat{\mathbf{y}}_k = \Theta\hat{\mathbf{x}}_k. \tag{21}$$

IV. Multiple Model Dynamic Mode Decomposition Flowfield Estimation

In this section, we present the main contribution of this work: the extension of the DMD-based flowfield estimation from systems with fixed model parameters (sufficiently described by a single DMD model) to systems with varying

model parameters, where a single set of DMD modes is not enough to describe the flow structures at significantly different model parameters (e.g. Reynolds number or angle of attack). This extension leverages the concept of MMKF, first introduced in [30], to balance the contribution of each DMD model to the full flowfield estimate.

Assume that the dynamics of the high-dimensional system depend on a generally unknown vector or scalar parameter $m \in \mathcal{M} \subseteq \mathbb{R}^d$. In this case, the discrete-time dynamics can be written as

$$\mathbf{y}_{k+1} = \mathbf{f}(\mathbf{y}_k; m). \tag{22}$$

In the simplest case, m is a constant. However, we can also allow m to vary *slowly* in time.

Assume that we also have M sets of measurements

$$\mathcal{D}_i = \{(\mathbf{y}^{(j)}, \mathbf{f}(\mathbf{y}^{(j)}; m_i) : \ j = 1, \dots, p\}, \tag{23}$$

for $i = 1, \dots, M$, of the high-dimensional system, obtained for different values of the parameter $m = m_i$, for $i = 1, \dots, M$. For instance, if the system of interest is the flow around a flat plate, the system parameter m could be the angle of attack and $\mathcal{D}_i$ the flowfield measurements at a given angle m_i. Note that m_i does not necessarily have to be a discrete (constant) value, but it can also belong to a subset $\mathcal{M}_i \subset \mathcal{M}$ of the parameter space (e.g. a range of angles of attack).

For each of the discrete parameters m_i, we fit a sparse DMD model on the corresponding data set $\mathcal{D}_i$, resulting in a *bank* of DMD models

$$\mathbf{x}_{k+1}^{(i)} = A^{(i)}\mathbf{x}_k^{(i)} + \mathbf{w}_k^{(i)}, \quad \mathbf{w}_k^{(i)} \sim \mathcal{N}(0, Q^{(i)}), \tag{24}$$

$$\mathbf{y}_k = \Theta^{(i)}\mathbf{x}_k^{(i)} + \boldsymbol{\epsilon}_k^{(i)}, \quad \boldsymbol{\epsilon}_k^{(i)} \sim \mathcal{N}(0, \Sigma^{(i)}), \tag{25}$$

$$\mathbf{z}_k = C^{(i)}\mathbf{x}_k^{(i)} + \mathbf{v}_k^{(i)}, \quad \mathbf{v}_k^{(i)} \sim \mathcal{N}(0, R^{(i)}), \tag{26}$$

for $i = 1, \dots, M$, where $\mathbf{x}_k^{(i)}$ is the state of the reduced-order model for $m = m_i$ and $(A^{(i)}, \Theta^{(i)}, C^{(i)})$ are computed using sparsity-promoting DMD and determine the evolution of the reduced-order state ($A^{(i)}$) and the mappings from the low-dimensional state space to the full flowfield ($\Theta^{(i)}$) and the real-time measurements ($C^{(i)}$).

Our goal is to estimate the flowfield $\mathbf{y}_k$ given a history of measurements, $Z^k = \{\mathbf{z}_j : j = 1, \dots, k\}$, and the bank of DMD models, *when the model parameter m is unknown*. If we knew that m is equal to one of the parameters for which we have a DMD model, then we could simply select the appropriate DMD model and perform the flowfield estimation as described in Section III. However, when m is *unknown* or *not one of the training values* m_i, we have to either select the most appropriate DMD model or utilize the estimates from each model. In particular, under the *Multiple Model Kalman Filter* (MMKF) framework, we can estimate the flowfield in a minimum mean-squared error (MMSE) sense using the probabilities of each model being the correct to weight the contribution from each model as

$$\hat{\mathbf{y}}_k^{\text{MMSE}} = \sum_{i=1}^{M} \mu_k^{(i)} \Theta^{(i)} \hat{\mathbf{x}}_k^{(i)}, \tag{27}$$

where

$$\mu_k^{(i)} = p(m = m_i \mid Z^k) \tag{28}$$

is the probability of the i-th model being correct given the available measurements and $\hat{\mathbf{x}}_k^{(i)} = \mathbb{E}\left[\mathbf{x}_k^{(i)} \mid Z^k\right]$ is the state estimate for the i-th model, which is obtained by running a Kalman Filter for the individual model i.

The estimated probabilities $\mu_k^{(i)}$ can change at each time step as new measurements $\mathbf{z}_k$ become available. Using Bayes' rule, we can update $\mu^{(i)}$ recursively as

$$\begin{aligned}
\mu_k^{(i)} &= p(m = m_i \mid Z^k) \\
&= p(m = m_i \mid \mathbf{z}_k, Z^{k-1}) \\
&= \frac{p(\mathbf{z}_k \mid m = m_i, Z^{k-1}) p(m = m_i \mid Z^{k-1})}{p(\mathbf{z}_k \mid Z^{k-1})} \\
&= \frac{p(\mathbf{z}_k \mid m = m_i, Z^{k-1}) \mu_{k-1}^{(i)}}{\sum_{j=1}^{M} p(\mathbf{z}_k \mid m = m_j, Z^{k-1}) \mu_{k-1}^{(j)}},
\end{aligned} \tag{29}$$

where the likelihood $p(\mathbf{z}_k \mid m = m_i, Z^{k-1})$ can be computed from the KF of the i-th model as

$$p(\mathbf{z}_k \mid m = m_i, Z^{k-1}) = \mathcal{N}(\nu_k^{(i)}; 0, S_k^{(i)}), \tag{30}$$

where $\nu_k^{(i)} = \mathbf{z}_k - C^{(i)}\hat{\mathbf{x}}_k^{-(i)}$ is the innovation of the i-th KF at time step k and $S_k = C^{(i)}P_k^{-(i)}C^{(i)\top} + R^{(i)}$ is the innovation covariance. Note that $\sum_{i=1}^{M} \mu_k^{(i)} = 1$.

An important observation is that we cannot compute the MMSE estimate of the reduced-order state $\hat{\mathbf{x}}_k^{(i)}$ as we do for the full state in Eq. 27, since the reduced-order state of each model corresponds to a different set of DMD modes computed on a different dataset and cannot be summed as in Eq. 27. Following that observation, the different models can have a different number of DMD modes (n_x), depending on the specific dataset that each model is trained on.

V. Numerical Examples

In this section, we demonstrate the multiple model approach to flowfield estimation in simple flow settings where our goal is to estimate the flowfield from limited measurements in: 1) a Blasius boundary layer with a varying adverse pressure gradient (APG) and 2) the flow around a flat plate at varying angles of attack (AoA). High-fidelity direct numerical simulations (DNS) of a uniform laminar flow are performed using an in-house code based on [33] that solves the 3D Navier-Stokes equations via a pseudo-spectral algorithm [34] that includes a custom force field. Solid surface boundary conditions are imposed via immersed boundary forces. Note that in both cases we assume that *the full flowfield is available at training time, but only limited measurements are available at test time*.

A. Blasius Boundary Layer with Varying Adverse Pressure Gradient

Consider a 2D laminar boundary layer with a negative pressure gradient ($dp/dx < 0$). For a weak APG, the flow is steady (i.e. a single DMD mode is enough to describe the flow). As the magnitude of the APG increases, the flow separates and sheds vortices periodically. Assume that the pressure gradient is the unknown model parameter m. The Reynolds number is $Re = 1400$ based on the boundary layer thickness at the start of the computational domain. We record a snapshot of the vorticity field every 5 time steps of the DNS at an orthogonal grid of size 141×39 along the boundary layer. In total, the flowfield $\mathbf{y}$ consists of the vorticity at $n_y = 5499$ grid points. We collect snapshots for four different (suitably normalized) pressure gradients $m = dp/dx$:

- $m_1 = -12 \times 10^{-3}$
- $m_2 = -16 \times 10^{-3}$
- $m_3 = -20 \times 10^{-3}$
- $m_4 = -24 \times 10^{-3}$

For each parameter, a total of $p = 10000$ snapshots are collected with a normalized time step of $T_s = 6.25 \times 10^{-3}$ non-dimensionalized time units, forming the datasets $\mathcal{D}_i$, $i = 1, 2, 3, 4$.

A sparse DMD model is trained on each dataset, leading to a total of $M = 4$ models – one for each discrete value of the APG. Once the models are computed, we want to estimate the entire flowfield from limited wall measurements of vorticity. In particular, we use a set of $n_z = 5$ near-wall vorticity measurements (sampled at the same rate as the snapshots) to infer the rest of the flowfield, while the APG is *unknown* at test time.

1. System identification using sparsity-promoting DMD

Each sparse DMD model is trained on one of the datasets. Initially, we keep enough POD modes to capture the training snapshots with more than 99% accuracy (in the $\mathcal{L}_2$-norm sense). Then, we run sparsity-promoting DMD for a range of different parameters ρ and retain the 5, 25, 55, and 55 most important DMD modes for the 1st, 2nd, 3rd, and 4th model, respectively. This choice leads to a reconstruction error of the training snapshots of less than 1% (smaller APGs need less modes for the same accuracy). The bank of sparse DMD models consists of $\{(A^{(i)}, \Theta^{(i)}, C^{(i)})\}$, for each parameter m_i, $i = 1, 2, 3, 4$. In addition, for each model we estimate the covariances $Q^{(i)}$ (process noise) and $R^{(i)}$ (measurement noise) from the training data, according to Section III. Note that all the pairs $(A^{(i)}, C^{(i)})$, $i = 1, 2, 3, 4$, are observable.

2. Estimating the flowfield at an unknown pressure gradient.

We start a new simulation of the 2D Blasius boundary layer at a pressure gradient of $dp/dx = -20 \times 10^{-3}$, but this time we only measure the vorticity at the $n_z = 5$ locations near the wall. Our goal is to infer both the pressure gradient

and the rest of the vorticity field from those measurements. This is a parameter that is included in the training data. A bank of Kalman Filters – one for each DMD model – is initialized with $\hat{\mathbf{x}}_0^{(i)} = 0$ and $P_0^{(i)} = 100 I_{n_x}$ for $i = 1, 2, 3, 4$. Each KF runs separately and estimates the reduced-order state, $\mathbf{x}_k$, for each DMD model. The model probabilities are initialized equally, i.e. $\mu_0^{(i)} = 1/M$, where $M = 4$ is the total number of DMD models. Furthermore, additive zero-mean, Gaussian noise with standard deviation $\sigma_z = 0.01$ is added to the wall measurements, in order to test the robustness of the MMKF. The model probabilities $\mu_k^{(i)}$ are updated according to Eq. (29) with each new measurement (Figure 1a). At each time step, we also compute the estimation error as

$$e_k = \|\hat{\mathbf{y}}_k^{\text{MMSE}} - \mathbf{y}_k\|_2 / \|\mathbf{y}_k\|_2 \times 100. \tag{31}$$

Note that since the state $\mathbf{x}^{(i)}$ of each DMD model is, in general, a different quantity due to the data-driven nature of DMD, we can only obtain MMSE estimates of $\mathbf{y}$, since the quantities being summed in Eq. (27) are all the same physical quantities, i.e. vorticity at the same locations.

3. Discussion

The MMKF quickly chooses the correct model (Figure 1b) and the estimation error drops to less than 6% after 500 time steps (Figure 1c, black). The boundary layer at this APG is characterized by vortex shedding that weakens with time. While this is a simple flow setting, a large number of DMD modes (55) is needed to describe the flowfield for the larger APGs (3rd and 4th models) with an accuracy of more than 99% (in the $\mathcal{L}_2$-norm sense for the training data). When the data from all four different pressure gradients are combined and used in a single DMD model, the lack of robustness becomes more apparent. In the single model case, as the number of DMD modes increases, the error also tends to increase. This is due to the lack of observablility of the larger models. In particular, the DMD model with 25 modes is fully observable, while the larger models with 35 and 45 modes have 1 and 4 unobserved modes, respectively.

B. Flat Plate at a Varying Angle of Attack

Consider the 2D flow around a flat plate at different AoA. The flow is dominated by the periodic wake behind the flat plate. The angle of attack is considered as the model parameter, m, while the Reynolds number is constant and equal to $Re = 250$ (based on the chord length). Every 5 time steps of the DNS, we record a snapshot of the vorticity field at an orthogonal grid of size 231×135 around the flat plate for different model parameters m. In total, the flowfield $\mathbf{y}$ consists of the vorticity at $n_y = 31185$ grid points.

First, the flowfield snapshots are split in three separate datasets, each corresponding to a different subspace of the parameter space. In particular,

- $m_1 = 20^o$ (constant AoA)
- $m_2 \in (20^o, 30^o)$ (varying AoA)
- $m_3 = 30^o$ (constant AoA)

For each model parameter case, we collect $p = 2000$ pairs of snapshots with a time step of $T_s = 6.25 \times 10^{-3}$ non-dimensionalized time units, forming three datasets $\mathcal{D}_i$, $i = 1, 2, 3$.

Then, a sparse DMD model is trained on each dataset, for a total of $M = 3$ models. Once the models are computed, the goal is to estimate in real time the full flowfield from *limited* sensor measurements. In particular, we choose to place three sensors that measure the vorticity at three points in the wake of the flat plate and then estimate the rest of the flowfield using these three measurements and the DMD models. However, since we don't know the model parameter (i.e. the AoA) at test time, we cannot select a model by hand. Instead, we will infer the most appropriate model from the bank of DMD models using the Multiple Model Kalman Filter.

1. System identification using sparsity-promoting DMD

For each dataset, we train a sparse DMD model. In particular, we first keep enough POD modes to capture the training snapshots with more than 99% accuracy (in the $\mathcal{L}_2$-norm sense). Then, we run sparsity-promoting DMD and retain the 25 most important DMD modes for the 1st and 3rd model ($m = 20^o$ and $m_{=}30^o$) and 45 DMD modes for the 2nd model ($m \in (20^o, 30^o)$). The bank of sparse DMD models consists of $\{(A^{(i)}, \Theta^{(i)}, C^{(i)})\}$, for each parameter m_i, $i = 1, 2, 3$. In addition, for each model we estimate the covariances $Q^{(i)}$ (process noise) and $R^{(i)}$ (measurement noise) from the training data, according to Section III. Comparisons are performed with a *single* DMDsp model trained on the combined datasets $\mathcal{D}_1 \cup \mathcal{D}_2 \cup \mathcal{D}_3$ and with different number of DMD modes.

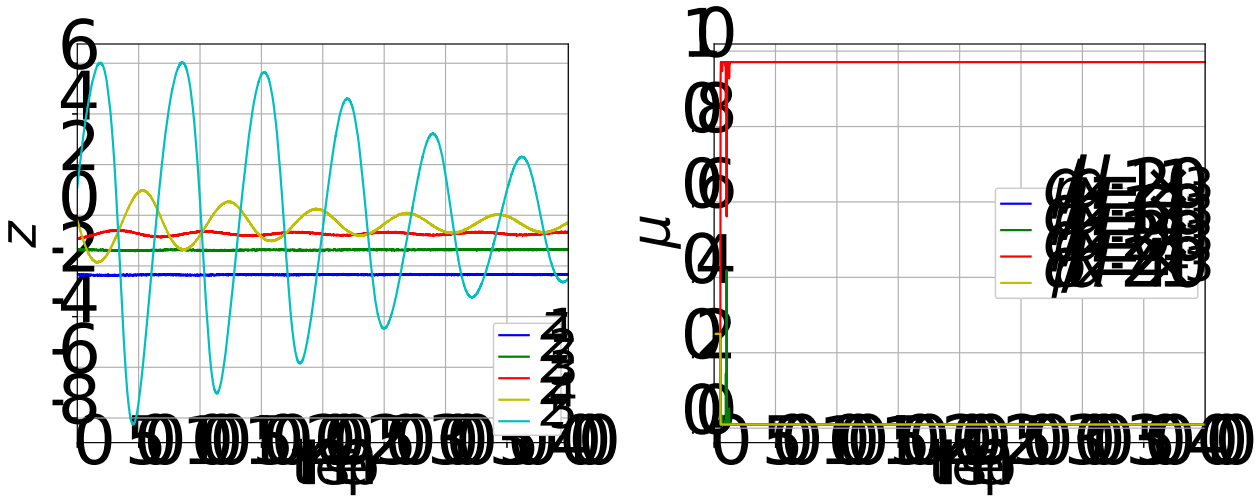

(a) Near-wall vorticity measurements obtained from a DNS of a Blasius boundary layer at $dp/dx = -20 \times 10^{-3}$.

(b) Probabilities of each model being correct, given the noisy measurements.

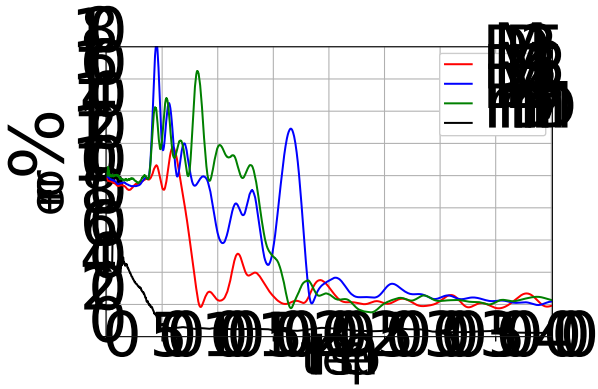

(c) Estimation error, E_k, at each time step, for the MMSE estimate of y. The multiple model DMD estimation error (black) is compared with the single-DMD-model estimation error for different DMD model sizes. Estimation error of standard DMD increases with model size due to lack of observability.

Fig. 1 2D Blasius boundary layer at an adverse pressure gradient. While the MMKF initially has a hard time choosing a model, after a while it converges to the correct model choice (3rd model).

2. Estimating the flowfield at varying AoA

We start a DNS of the flat plate at $m = 20^o$ for 2000 time steps. Then, the flat plate rotates to $m = 30^o$ at a constant rate for 1000 time steps and stays at that angle for another 5000 steps. The goal is to estimate the flowfield throughout the simulation just by measuring the vorticity at only three points at the wake of the flat plate. Artificial (zero mean, Gaussian) noise with standard deviation $\sigma_z = 0.05$ is also added to the measurements. We initialize the bank of Kalman Filters – one for each DMD model – with $\hat{\mathbf{x}}_0^{(i)} = 0$ and $P_0^{(i)} = 100 I_{n_x}$ for $i = 1, 2, 3$. Each KF runs separately and estimates the reduced-order state, $\mathbf{x}_k$, for each DMD model. In addition, the model probabilities are initialized equally, i.e. $\mu_0^{(i)} = 1/M$, where $M = 3$ is the total number of DMD models. Here, the model probabilities are kept constant for the first 50 time steps, until the individual KFs have started converging to more realistic state estimates. Then, probabilities $\mu_k^{(i)}$ are updated according to Eq. (29). At each time step, we also compute the estimation error of the MMSE estimates of $\mathbf{y}$, as in the previous example.

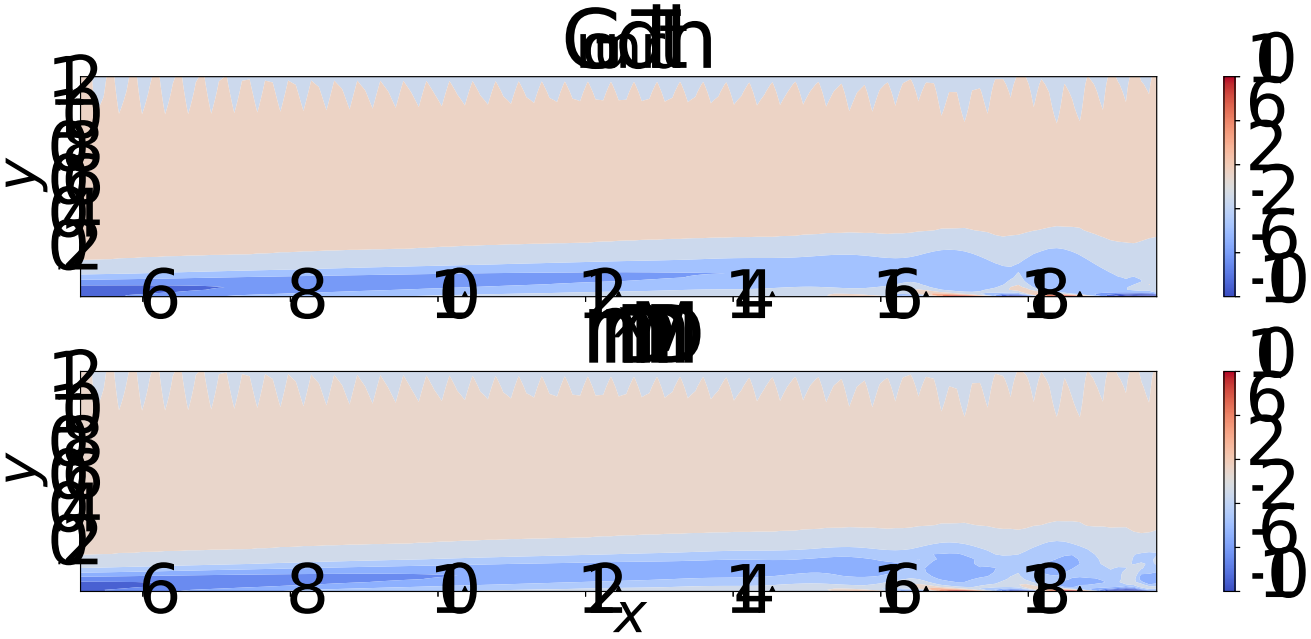

(a) Flowfield at time step $k = 1000$.

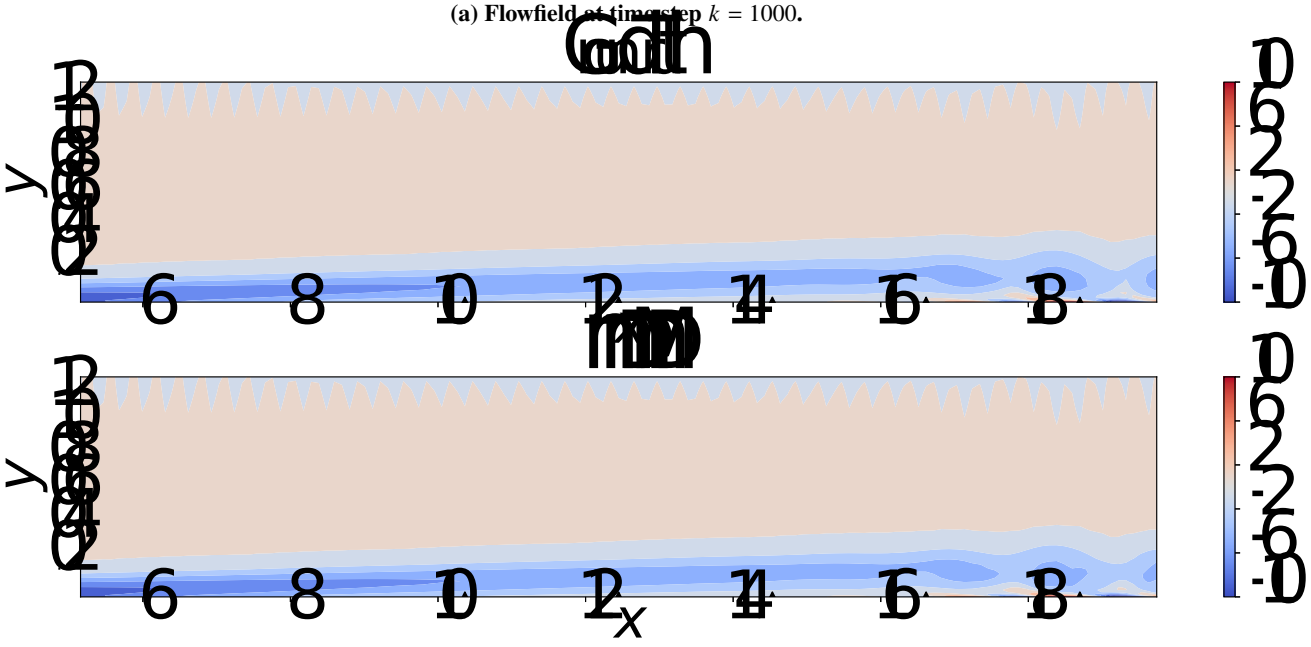

(b) Flowfield at time step $k = 1000$.

Fig. 2 Actual (top) vs estimated (bottom) flowfield of the 2D Blasius boundary layer at an adverse pressure gradient of $dp/dx = -20 \times 10^{-3}$ (non-dimensionalized). In both cases, the estimator yields an error of less than 10%. Measurement positions are shown as black triangles near the wall.

3. Discussion

During the first few time steps, the MMKF is still figuring out which model best fits the noisy measurements (Figure 3a), as indicated by the model probabilities (Figure 3b). After a while, the estimator correctly selects the model with $m = 20^o$, leading to $\mu_1 \rightarrow 1$, while the other probabilities go to zero. At the same time, once the MMKF selects the appropriate model, the estimation error also reduced to less than 10% (Figure 3c). Once the flat plate starts rotating (around $k = 2000$), the estimator switches to the 2^{nd} model, which was trained on an AoA varying within $m \in (20^o, 30^o)$ and captures the modes of the rotating plate. The estimator then switches to the 3^{rd} model ($m = 30^o$) just after the AoA stabilizes at 30^o. Note that the model probabilities initially appear to be noisy due to the smaller signal-to-noise ratio caused by the added measurement noise (which has a constant standard deviation).

While the AoA is constant, the estimation error converges to below 10% as more measurements are collected. The model has a harder time estimating the flowfield when the (unknown) AoA starts increasing. However, the error still remains at a qualitatively acceptable value below 20% (Figure 3c, black). For comparison, single-DMD-model estimation is performed for a DMD model trained on the entire dataset with 25 and 45 DMD modes. The larger DMD model captures the training data with more than 97.5% accuracy. While both models perform similarly to mmDMD when the AoA is varying, they perform worse when the AoA is constant (Figure 3c, blue and red). One of the reasons for the estimation error not further decreasing with more DMD modes is the lack of observability which is noticed with increasing model size. However, with the multiple DMD models, we are able to capture subspaces of the parameter space with fewer DMD modes, while the model remains observable.

The convergence of the filter toward the actual flowfield can also be seen by visualizing the actual vorticity field at different time steps and comparing it with the estimated one (top and bottom of Figure 4, respectively). At both 20^o (Figure 4a) and 30^o (Figure 4b), the flowfield is qualitatively similar to the ground truth (i.e. the DNS simulation).

VI. Conclusion

In this work, we presented a framework for flowfield estimation in settings with unknown model parameters using a "bank" of Dynamic Mode Decomposition models under the multiple model Kalman filter framework. The advantage of the proposed method is the ability of the estimator to infer the unknown model parameters, such as the angle of attack of a flat plate or the pressure gradient of a boundary layer, from limited flow measurements. In addition, splitting the datasets in smaller subsets based on the model parameters leads to smaller and more accurate models (that remain observable), suitable for flowfield estimation. Future work includes using the proposed estimator in closed-loop flow control settings.

Acknowledgements

This research has been supported in part by NSF-CBET, award # 2129494, and NSF-CMMI, award # 2052811. The authors acknowledge the Texas Advanced Computing Center (TACC) at The University of Texas at Austin for providing HPC resources that have contributed to the research results reported within this paper. Alexandros Tsolovikos acknowledges support by the A. Onassis Foundation Scholarship.

References

[1] Kim, J., and Bewley, T. R., "A linear systems approach to flow control," *Annu. Rev. Fluid Mech.*, Vol. 39, 2007, pp. 383–417.

[2] Rowley, C. W., and Dawson, S. T., "Model reduction for flow analysis and control," *Annual Review of Fluid Mechanics*, Vol. 49, 2017, pp. 387–417.

[3] Lumey, J. L., *Stochastic Tools in Turbulence.*, Elsevier Science, 1970.

[4] Willcox, K., and Peraire, J., "Balanced model reduction via the proper orthogonal decomposition," *AIAA journal*, Vol. 40, No. 11, 2002, pp. 2323–2330.

[5] Juang, J.-N., Phan, M., Horta, L. G., and Longman, R. W., "Identification of observer/Kalman filter Markov parameters-Theory and experiments," *Journal of Guidance, Control, and Dynamics*, Vol. 16, No. 2, 1993, pp. 320–329.

[6] Schmid, P. J., "Dynamic mode decomposition of numerical and experimental data," *Journal of Fluid Mechanics*, Vol. 656, 2010, pp. 5–28.

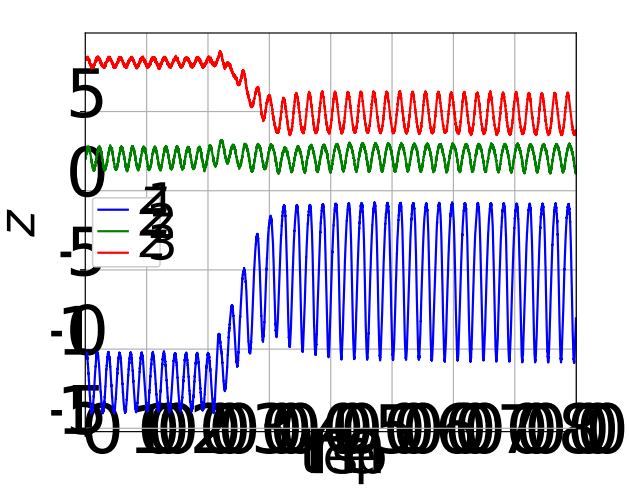

(a) Noisy measurements obtained from a DNS of the flat plate at an AoA varying from $m = 20^o$ to $m = 30^o$.

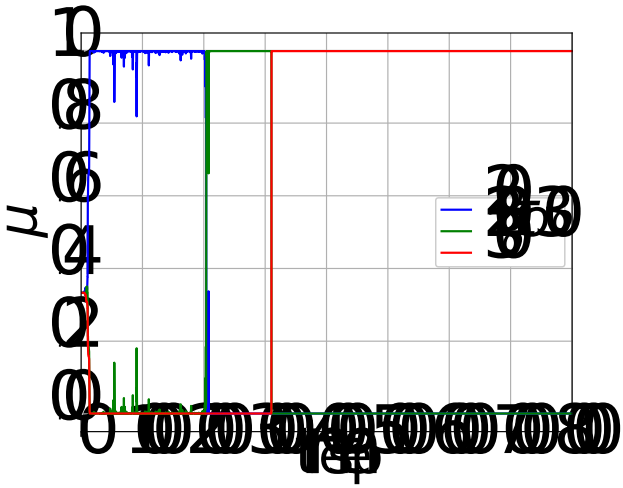

(b) Probabilities of each model being correct, given the noisy measurements.

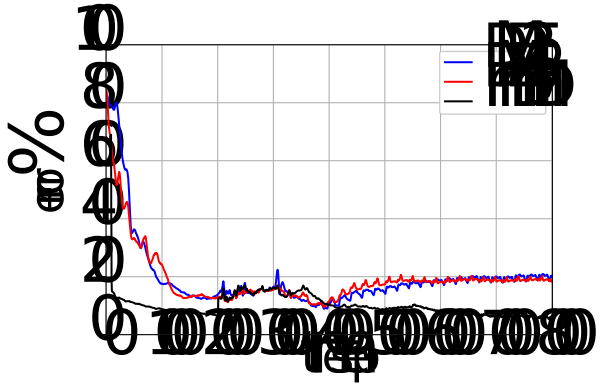

(c) Estimation error, E_k, at each time step, for the MMSE estimate of y. The multiple model DMD estimation error (black) is compared with the single-DMD-model estimation error for different DMD model sizes.

Fig. 3 Flat plate at varying AoA. The MMKF initially selects the 1st DMD model ($m = m_1$), then identifies that the AoA starts increasing ($m \in m_2$), and finally settles at the 3rd DMD model ($m = m_3$).

[7] Rowley, C. W., Mezić, I., Bagheri, S., Schlatter, P., and Henningson, D. S., "Spectral analysis of nonlinear flows," *Journal of Fluid Mechanics*, Vol. 641, 2009, pp. 115–127.

[8] Proctor, J. L., Brunton, S. L., and Kutz, J. N., "Dynamic mode decomposition with control," *SIAM Journal on Applied Dynamical Systems*, Vol. 15, No. 1, 2016, pp. 142–161.

[9] Sirovich, L., "Turbulence and the dynamics of coherent structures. I. Coherent structures," *Quarterly of Applied Mathematics*, Vol. 45, No. 3, 1987, pp. 561–571.

[10] Ma, Z., Ahuja, S., and Rowley, C. W., "Reduced-order models for control of fluids using the eigensystem realization algorithm," *Theoretical and Computational Fluid Dynamics*, Vol. 25, No. 1-4, 2011, pp. 233–247.

[11] Alfatlawi, M., and Srivastava, V., "An incremental approach to online dynamic mode decomposition for time-varying systems with applications to EEG data modeling," *arXiv preprint arXiv:1908.01047*, 2019.

[12] Hemati, M. S., Rowley, C. W., Deem, E. A., and Cattafesta, L. N., "De-biasing the dynamic mode decomposition for applied Koopman spectral analysis of noisy datasets," *Theoretical and Computational Fluid Dynamics*, Vol. 31, No. 4, 2017, pp. 349–368.

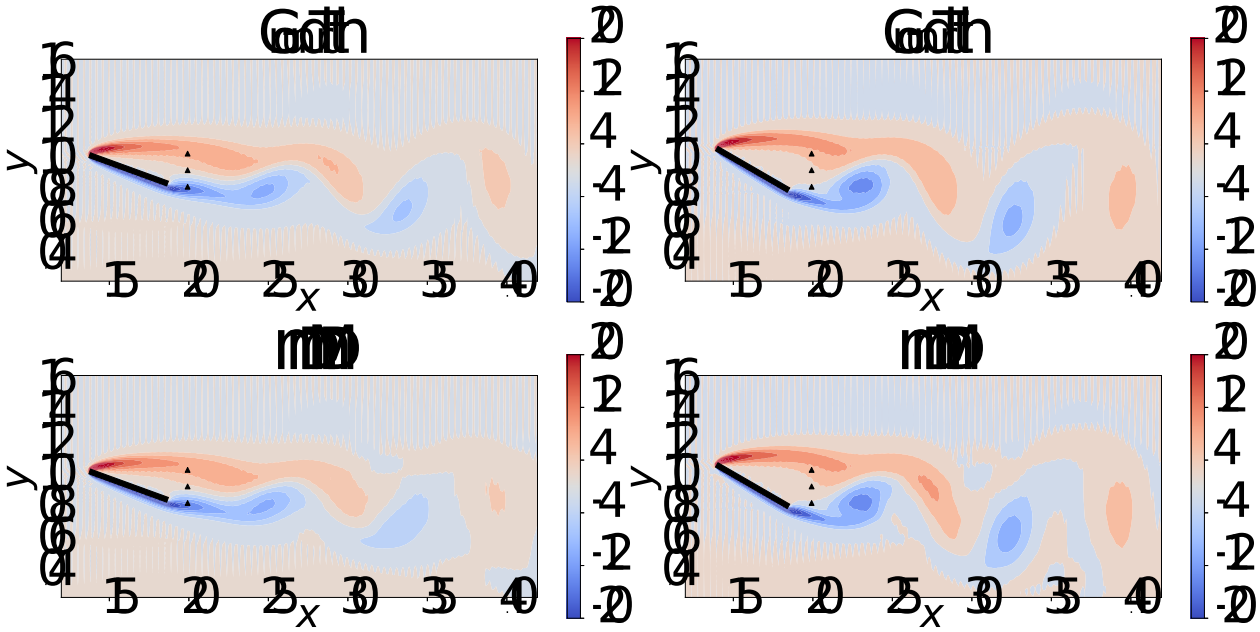

(a) Flowfield at time step $k = 1500$ and $m = 20^o$. **(b) Flowfield at time step $k = 5000$ and $m = 30^o$.**

Fig. 4 Actual (top) vs estimated (bottom) flowfield around the flat plate. In both cases, the estimator yields an error of less than 10%. Measurement locations are shown as triangles at the wake of the flat plate.

[13] Dawson, S. T., Hemati, M. S., Williams, M. O., and Rowley, C. W., "Characterizing and correcting for the effect of sensor noise in the dynamic mode decomposition," *Experiments in Fluids*, Vol. 57, No. 3, 2016, p. 42.

[14] Hemati, M. S., Williams, M. O., and Rowley, C. W., "Dynamic mode decomposition for large and streaming datasets," *Physics of Fluids*, Vol. 26, No. 11, 2014, p. 111701.

[15] Takeishi, N., Kawahara, Y., Tabei, Y., and Yairi, T., "Bayesian Dynamic Mode Decomposition." *IJCAI*, 2017, pp. 2814–2821.

[16] Mezić, I., "Analysis of fluid flows via spectral properties of the Koopman operator," *Annual Review of Fluid Mechanics*, Vol. 45, 2013, pp. 357–378.

[17] Williams, M. O., Kevrekidis, I. G., and Rowley, C. W., "A data–driven approximation of the koopman operator: Extending dynamic mode decomposition," *Journal of Nonlinear Science*, Vol. 25, No. 6, 2015, pp. 1307–1346.

[18] Takeishi, N., Kawahara, Y., and Yairi, T., "Learning Koopman invariant subspaces for dynamic mode decomposition," *arXiv preprint arXiv:1710.04340*, 2017.

[19] Chen, K. K., Tu, J. H., and Rowley, C. W., "Variants of dynamic mode decomposition: boundary condition, Koopman, and Fourier analyses," *Journal of Nonlinear Science*, Vol. 22, No. 6, 2012, pp. 887–915.

[20] Wynn, A., Pearson, D., Ganapathisubramani, B., and Goulart, P. J., "Optimal mode decomposition for unsteady flows," *Journal of Fluid Mechanics*, Vol. 733, 2013, pp. 473–503.

[21] Jovanović, M. R., Schmid, P. J., and Nichols, J. W., "Sparsity-promoting dynamic mode decomposition," *Physics of Fluids*, Vol. 26, No. 2, 2014, p. 024103.

[22] Annoni, J., Seiler, P., and Jovanović, M. R., "Sparsity-promoting dynamic mode decomposition for systems with inputs," *2016 IEEE 55th Conference on Decision and Control (CDC)*, IEEE, 2016, pp. 6506–6511.

[23] Tu, J. H., Rowley, C. W., Luchtenburg, D. M., Brunton, S. L., and Kutz, J. N., "On dynamic mode decomposition: Theory and applications," *arXiv preprint arXiv:1312.0041*, 2013.

[24] Tsolovikos, A., Bakolas, E., Suryanarayanan, S., and Goldstein, D., "Estimation and Control of Fluid Flows Using Sparsity-Promoting Dynamic Mode Decomposition," *IEEE Control Systems Letters*, Vol. 5, No. 4, 2020, pp. 1145–1150.

[25] Tsolovikos, A., Suryanarayanan, S., Bakolas, E., and Goldstein, D., "Model Predictive Control of Material Volumes with Application to Vortical Structures," *AIAA Journal*, Vol. 59, No. 10, 2021, pp. 4057–4070.

[26] Gomez, D. F., Lagor, F. D., Kirk, P. B., Lind, A. H., Jones, A. R., and Paley, D. A., "Data-driven estimation of the unsteady flowfield near an actuated airfoil," *Journal of Guidance, Control, and Dynamics*, Vol. 42, No. 10, 2019, pp. 2279–2287.

[27] Nonomura, T., Shibata, H., and Takaki, R., "Dynamic mode decomposition using a Kalman filter for parameter estimation," *AIP Advances*, Vol. 8, No. 10, 2018, p. 105106.

[28] Nonomura, T., Shibata, H., and Takaki, R., "Extended-Kalman-filter-based dynamic mode decomposition for simultaneous system identification and denoising," *PloS one*, Vol. 14, No. 2, 2019, p. e0209836.

[29] Surana, A., and Banaszuk, A., "Linear observer synthesis for nonlinear systems using Koopman operator framework," *IFAC-PapersOnLine*, Vol. 49, No. 18, 2016, pp. 716–723.

[30] Magill, D., "Optimal adaptive estimation of sampled stochastic processes," *IEEE Transactions on Automatic Control*, Vol. 10, No. 4, 1965, pp. 434–439.

[31] Bar-Shalom, Y., Li, X. R., and Kirubarajan, T., *Estimation with applications to tracking and navigation: theory algorithms and software*, John Wiley & Sons, 2004.

[32] Candes, E. J., Wakin, M. B., and Boyd, S. P., "Enhancing sparsity by reweighted L1 minimization," *Journal of Fourier Analysis and Applications*, Vol. 14, No. 5-6, 2008, pp. 877–905. https://doi.org/10.21236/ada528514.

[33] Goldstein, D., Handler, R., and Sirovich, L., "Modeling a no-slip flow boundary with an external force field," *Journal of Computational Physics*, Vol. 105, No. 2, 1993, pp. 354–366.

[34] Kim, J., Moin, P., and Moser, R., "Turbulence statistics in fully developed channel flow at low Reynolds number," *Journal of Fluid Mechanics*, Vol. 177, 1987, pp. 133–166.